Chapter

High-k, Low-Loss Ceramic-Thermoplastic Composite Feedstock Filaments for Fused Deposition Modeling of Microwave and mm-Wave Devices

Vishvajitsinh Kosamiya and Jing Wang

Abstract

Maturing of additive manufacturing (AM) techniques has increased their utilization for fabricating radio frequency (RF) and microwave devices. Solid composites used in material extrusion AM have experienced considerable expansion over the past decade, incorporating functional properties into 3D-printed objects. There are encouraging indications from AM material research that electrically efficient AM materials can be discovered. These materials would be useful for producing microwave components in the future. One of the enabling techniques for fabricating these materials is to incorporate nano/microparticles or fillers into thermoplastic material. Composite material 3D printing is a novel approach to managing materials' microwave properties. While extrinsic qualities (effective permittivity) can be controlled by shape and porosity management, intrinsic attributes are tied to the composition of composites. Furthermore, combining various materials to increase the spectrum of available microwave characteristics is made possible by multi-material 3D printing. In this chapter, we explore different methodologies to fabricate ceramic/thermoplastic composites for fused deposition modeling (FDM) of RF and microwave devices. Analytical models for predicting effective permittivity of the composite are discussed and application examples of FDM printed RF, microwave and mm-wave devices employing composites are presented.

Keywords: ceramic-thermoplastic composite, fused deposition modeling, high-k low-loss dielectrics, dielectric constant, dielectric loss tangent

1. Introduction

Research on electromagnetic (EM) devices and microwave circuits has historically mostly focused on two-dimensional designs that complement established printed circuit board (PCB) technologies [1, 2]. Additive manufacturing (AM) has gained a lot of traction for creating small quantities of highly specialized devices, whereas printed

circuit board (PCB) technology has been thoroughly refined and optimized for mass-producing affordable consumer electronics products. Though it cannot fully replace traditional manufacturing for mass production, additive manufacturing (AM) presents a disruptive alternative in businesses that require high levels of design customization and small production volumes [3, 4].

In recent years, there has been a rise in study on AM in the field of electrical engineering [5–7]. By removing the limitations on possible shapes that were previously imposed by traditional production techniques, the third dimension made possible by AM provides substantial benefits [8–13]. Using a graded material (easier to produce using AM) to achieve a required EM response allows the geometry to be optimized for other reasons, such as aerodynamics. Some of the main types of 3D printing methods used for fabricating radio frequency (RF) and microwave components include fused deposition modeling (FDM) [14], poly-jet printing, stereolithographic apparatus (SLA) [15], selective laser sintering (SLS) [16] and selective laser melting (SLM) [17].

One popular AM method that is well-known for its ease of use and adaptability is FDM [18, 19]. This technique is fundamental to the field of 3D printing since it provides a useful and affordable way to bring complex ideas to life. In FDM process, the printer heats a material (thermoplastic or composites made from thermoplastic) above its glass transition temperature and then deposits it through a nozzle, building an object layer by layer, as shown in **Figure 1**. Although FDM has comparatively poor resolution control, it is compatibility with a wider range of available material and their composites makes it suitable for prototyping and experimenting with different varieties of recipes [5, 20, 21]. Furthermore, FDM is normally a single step process, not requiring and post-processing steps. Depending on the quality of the printer mechanics and the use of the proper printer settings, FDM can achieve a degree of precision of about 0.1 to 0.2 mm.

The FDM printers can have more than one extrusion nozzle to support printing of multi-material parts [22]. FDM can be considered as the most versatile AM technology for microwave component manufacturing. High design flexibility is made possible by

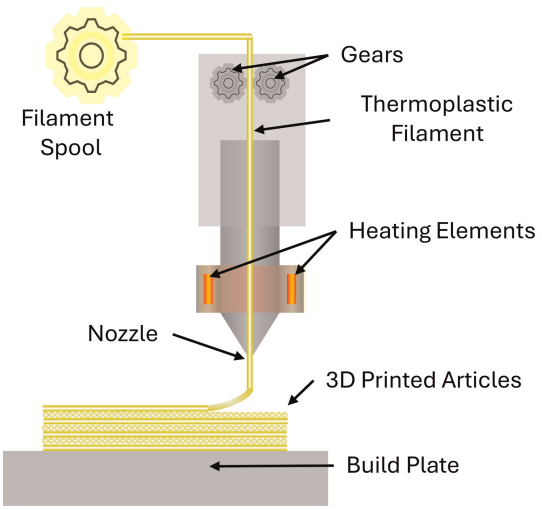

Figure 1.
Schematic representation of fused deposition modeling (FDM) process.

the substantial size of the FDM material catalog. Additionally, FDM prototyping is a popular option for RF engineers because of its inexpensive cost [23].

However, the possibility of creating extremely small devices is limited by the moderate dielectric constant ($\varepsilon_r \sim 2$–3) displayed by the most popular printable filaments, as well as the extra reduction brought on by the inevitable interstitial air gaps between the rods extruded during the printing process [24, 25]. For electronics engineering, especially RF and microwave devices permittivity of the material matters significantly because of its influence on guided wavelength inside the material, as seen in the following equation,

$$\lambda_g = \frac{c_0}{f\sqrt{\varepsilon_r}} \tag{1}$$

where λ_g is the guided wavelength, C_0 is the speed of light in vacuum. As Eq. (1) suggests that for a signal with a given frequency, higher permittivity material will cause it to have a smaller wavelength. This relation is widely adopted by antenna engineers to miniaturize antennas for RF and microwave applications [20, 26, 27]. At the microscopic level, several dielectric mechanisms can contribute to the dielectric constant of a given material [28]. Dipole orientation and ionic conduction interact strongly at microwave frequencies, as shown in **Figure 2**. For instance, water molecules rotate in response to an alternating electric field because they are permanent dipoles. Food warms in a microwave oven because these mechanisms are quite lossy. Over the microwave area, atomic and electronic mechanisms are typically constant and rather weak.

To increase low permittivity of common thermoplastic materials, researchers have come up with ways to disperse ceramic particles in thermoplastic matrix and utilize it to fabricate RF and microwave devices [5, 20, 21, 26, 29, 30]. This chapter is subdivided into five sections. Section I introduces relative permittivity of materials and why it matters to RF and microwave engineers as well as FDM process. Different fabrication methods of ceramic/thermoplastic composite filaments for FDM of RF and

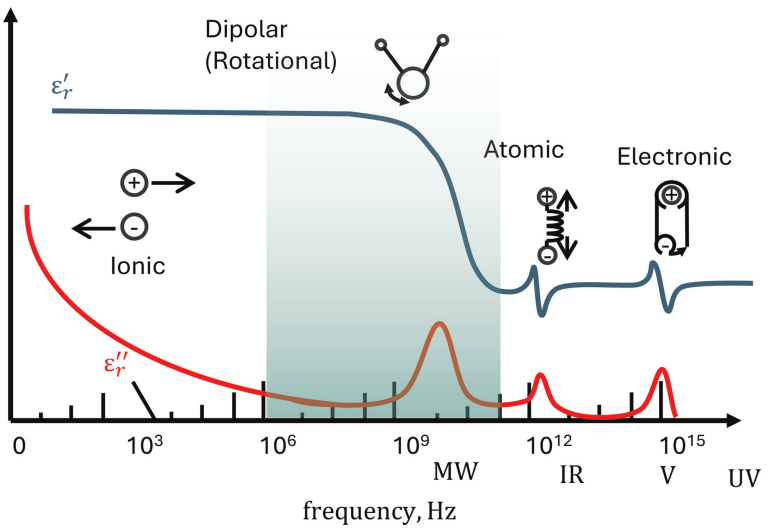

Figure 2.
Frequency responses of dielectric mechanisms [28]. The highlighted green area represents RF, microwave, and mm-wave frequency range.

microwave devices in literature are discussed in section II. Section III explores different analytical models available for prediction of the effective permittivity of a composite material based on permittivity values and volume fraction of constituent materials. Experimental demonstrations of microwave and mm-wave devices 3D printed using ceramic/thermoplastic feedstock filaments are discussed in section IV. Finally, section V presents concluding remarks and an outlook on future research in this topic.

2. Synthesis methods

Polymer-based composites can be used to combine the processability of the polymer matrix with the EM characteristics of discrete filler particles using predetermined mixing methods [31, 32]. For composites to act as a homogenous medium in terms of electromagnetic energy transmission, the wavelength inside the medium must be substantially larger than the scale of the particles or particle agglomerates [33, 34]. This condition can be easily met with well-dispersed particles of 10^{-6} to 10^{-4} m exposed to microwaves with free-space wavelengths higher than 10^{-2} m, resulting in non-resonant bulk materials appropriate for broadband applications.

Synthesis methods can be characterized based on the method of mixing the filler particles inside the thermoplastic matrix: (1) melt mixing (MM) and (2) solution-assisted dispersion (SD) [35, 36].

2.1 Melt mixing

This technique involves heating the thermoplastic matrix to its melting point, followed by the addition of filler particles to the semi-liquid thermoplastic and stirring with a mechanical screw [37], as illustrated in **Figure 3**. With an increase in filler particle volume, it becomes more difficult to distribute the filler particles in the melted polymer due to a decrease in the solution's viscosity. Melt mixing can produce consistent results for a filler volume fraction of 0.3 or less [31, 38–40]. Nevertheless, no additional chemicals are needed for this method, and process adjustments can be made as thermoplastic is being extruded in the FDM filament.

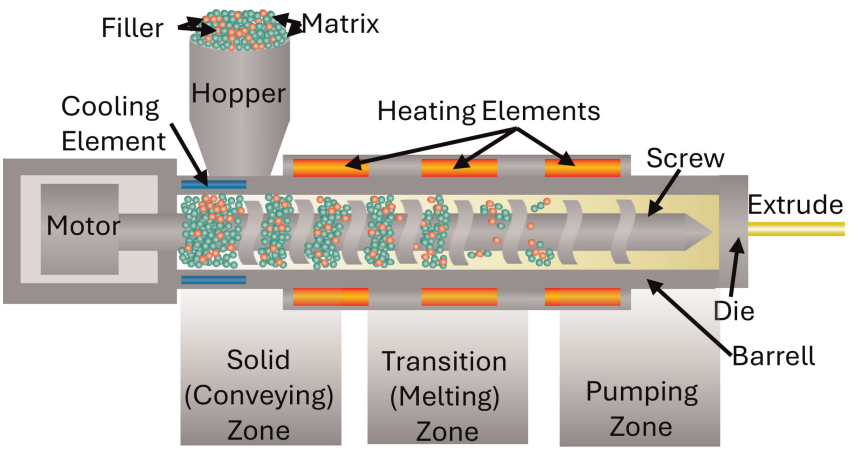

Figure 3.
Schematic representation of melt mixing process using a single screw extruder.

An extruder essentially consists of a steel screw that rotates inside a heated barrel, like an auger. Thermoplastic resin, in the form of pellets, is fed to the screw through a hopper, and the screw compacts, melts and pressurizes the polymer. After the tip of the screw, a die is attached to the barrel, and the high-pressure melt is forced through the die and extruded into desired shape. The screw has many functions, which include compressing the solid pellets, heating the resin through mechanical deformation, pressurizing the melt, and mixing. Using special screw geometries, mixing can be achieved on a single screw extruder, but it is generally recognized that the best mixing is achieved on twin screw extruders [37].

2.2 Solution assisted dispersion

The SD method is broken into multiple sub-steps: (i) agitation to disperse filler particles in a solvent, (ii) agitation to mix filler and polymer solutions, and (iii) controlled solvent evaporation and/or nanocomposite precipitation. The process diagram of the SD method is shown in **Figure 4**. In this method, the thermoplastic is first dissolved using a chemical solvent at room temperature, and then filler particles are added to liquid solution and stirred. After a homogeneous dispersion is achieved, the solvent is evaporated at 60°C to leave behind just the thermoplastic polymer and filler

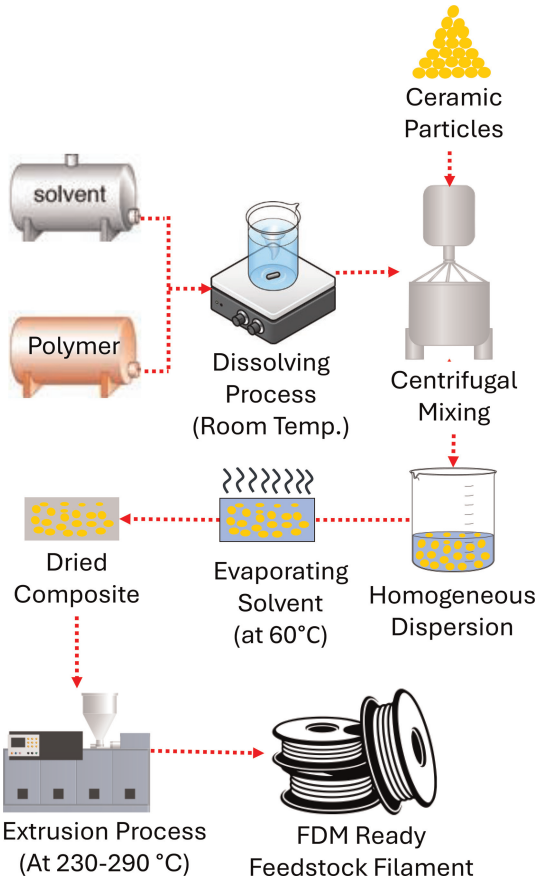

Figure 4.
Process flow diagram of solution-assisted dispersion (SD) method.

particles [21, 30, 41, 42]. This process used by authors in [43] with extrusion temperatures in the range of 230–290°C, can achieve repeatable results up to 50% filler volume concentration.

However, this process requires additional processing steps, and if the solvent is not reused, it could become expensive. Residual solvent inside final composite can also have a negative impact on the dielectric and loss properties of the composite. A key challenge is to keep the filler particles from agglomeration during the process of evaporating the solvent.

Both MM and SD methods could be modified by introducing a surfactant either during or before the mixing process [5, 21, 31, 43]. The surfactant could perform a dual function of improving the adhesion between filler and matrix as well as hindering the filler particles from agglomerating. Care must be taken to optimize the quantity of the surfactant to maintain both mechanical properties required for 3D printing as well as dielectric properties for EM applications [40, 41].

2.3 Examples of works in literature

Castles et al. [21] used the SD method to disperse $BaTiO_3$ (BT) particles in acrylonitrile butadiene styrene (ABS) matrix up to 29 vol% to achieve relative permittivity values in the range of 2.6–8.7 and loss tangents in the range 0.005–0.027. They also fabricated 1D and 2D periodic structures to demonstrate the feasibility of 3D printing; however, the EM functionalities of those prototypes were not discussed.

In a sequential study, Wu et al. [41] described the production of a better polymer-ceramic composite feedstock filament for utilization in FDM 3D printing. The preceding formulation was enhanced by adding a surfactant and plasticizer. The optimum ratio of surfactant and plasticizer was found by doing a parametric study of their effects on dielectric permittivity. Filament with a maximum solid loading of 32 vol% was manufactured; its dielectric permittivity and loss tangents measured at 15 GHz using a split post-dielectric resonator were found to be 11 and 0.0289, respectively.

Khatri et al. [40] also fabricated ABS-BT composite; however, they utilized the MM method to disperse BT particles in the ABS matrix. They also utilized 1.1 wt % steric acid as a surfactant to improve adhesion between inorganic filler and organic matrix. They obtained a relative permittivity of 11.5 for the composite containing 35 vol% BT. This study's findings were consistent with the Maxwell-Garnett [32, 44] and Jayasundere-Smith [45] mixing models.

To improve the overall dielectric loss tangent of composite feedstock, Castro et al. [29] used cyclo-olefin polymer (COP) due to its superb electromagnetic properties with $\boldsymbol{\varepsilon_r}\sim 2.3$ and tan $(\delta_d) < 0.0005$ at 17 GHz. They employed the MM method to disperse TiO_2, $MgCaTiO_2$ (MCT), and $Ba_{0.55}Sr_{0.45}TiO_3$ (BST) particles into COP matrix. They were able to achieve a relative permittivity value of 4.88 for dielectric composite with 25% volume loading of BST in COP with a low-loss tangent of 0.007 at 17 GHz. For composite with 30% volume loading of TiO_2, they were able to achieve a low-loss tangent of 0.0014 and permittivity of 4.57. One of the key differences was that they also performed co-firing of ceramic particles before dispersing them in COP matrix. This helped in increasing crystallinity of ceramic particles and hence improving loss performance of composite.

Czarny et al. [46] used cyclic olefin copolymer (COC) polymer ($\boldsymbol{\varepsilon_r}\sim 2.3$, tan $(\delta_d) \sim 1.10^{-3}$) and loaded by titanium oxide (TiO_2) ($\boldsymbol{\varepsilon_r}\sim 100$, tan $(\delta_d) < 1.10^{-4}$), at 36 vol%. This innovative thermoplastic composite material has a high permittivity of up to 9.2 and a low-loss tangent of 1.10^{-3} at 9.3GHz. They used spray-drying to

produce titanium oxide grains on a micrometer size. They also sintered (TiO_2) particles at the optimized temperature of 1100°C. However, they fail to mention the method that was used to disperse ceramic filler in thermoplastic matrix.

Mazzei Capote et al. [5] used the SD method to create ABS and BT-based composites, which included the use of a surfactant and a plasticizer to aid processing. The ABS-based composite contained 75% BT (nominally 35% by volume, based on density), 5% dibutyl phthalate, and 1% octyl gallate. They were able to obtain a record high permittivity value of 12.85 in the 10 to 12 GHz band. The composite had a high-loss tangent (tan (δ_d) = 0.046), perhaps due to ABS's poor loss attributes. They implemented the use of ABS-based composite in the manufacturing process of microwave photonic devices. They 3D printed a 2D photonic crystal and experimentally verified its transmission performance. Furthermore, a prototype 3D photonic crystal was also 3D printed; however, it had insufficient unit cells to function properly.

To the best of our knowledge, authors [30] used SD method for the first time to disperse BST, MCT and TiO_2 particles into COP matrix. We also employed silane surfactant to improve adhesion between inorganic filler and organic polymer. The maximum measured ceramic particle filler volume concentration of 50% resulted in relative permittivity values of up to 12.35 and a low-loss tangent of 0.003. Ceramic particles were co-fired before surfactant-assisted ball milling to improve their dielectric and loss properties. Two functional dielectric waveguides were fabricated and characterized using developed composite and commercial counterpart [43].

Table 1 summarizes the state-of-the-art works in literature for developing ceramic-thermoplastic feedstock filament with high-k, low-loss properties. As can be seen, that SD method generally allows for higher permittivity values due to homogeneous dispersion of ceramic particles in matrix compared to MM method.

3. Analytical model predictions

The emergence of RF and microwave communication necessitated the development of substrate materials with tailorable dielectric and mechanical properties. Traditional dielectric materials cannot meet new requirements, such as balanced dielectric characteristics and good mechanical flexibility, as electronics become more multi-functional, integrated, and miniaturized. As a result of their excellent processibility, flexibility, and dielectric qualities, high dielectric polymer composites have sparked widespread interest. As the interaction between EM energy and matter are heavily influenced by the compositions and internal structure of the material, the dielectric properties of the composite have a direct impact on all applications in electronics. Hence there has been much research throughout history toward tackling the problem of rationalizing and predicting electrical properties of composite materials.

Maxwell and Faraday first studied formulae for the permittivity of heterostructures in the mid-nineteenth century as part of their comprehensive electric and magnetic research [47]. The models currently in literature can be broadly characterized in two categories: (1) mixing rule and (2) effective medium theory (EMT). This chapter focuses on the various cases in which composite regions are large enough to contain macroscopic fields. The advanced models based on percolation theory and complex electrodynamic-based models are not discussed here, but interested readers can find relevant information in the references.

Ref.	Matrix	Filler	Filler Fraction	Mixing Method	Surface Modification Applied.	Permittivity @GHz	Loss tangent @GHz
[27]	COC	TiO_2	36 vol %	n/a	No	7.7@37.1GHz	0.001 @37.1GHz
[5]	ABS	$BaTiO_3$	35 vol %	SD	Yes	12.85@12 GHz	0.046 @12GHz
[42]	ABS	$BaTiO_3$ $SrTiO_3$ $Ba_{0.67}Sr_{0.33}TiO_3$	30 vol %	SD	Yes	8.39 8.18 8.02 @18-40GHz	0.016 <0.01 0.069 @18-40GHz
[38]	ABS	$CaCu_3Ti_4O_{12}$	40 wt %	MM	No	9.6@18GHz	0.0057 @18GHz
[43]	COP	TiO_2 (Fired 1100°C)	50 vol %	SD	Yes	12@16GHz	0.003 @16GHz
[30]	COP	$Ba_{0.55}Sr_{0.45}TiO_3$ (Fired 1100°C) $MgCaTiO_2$ (Fired 1100°C)	50 vol %	SD	Yes	8.46@16GHz 12.35@12GHz	0.0099 @16GHz 0.0033 @12GHz
[41]	ABS	$BaTiO_3$	32 vol %	SD	Yes	11@15GHz	0.03 @15GHz
[29]	COP	$MgCaTiO_2$ (Fired 1200°C) TiO_2 (Fired 1200°C)	30 vol %	MM	No	4.78 4.82 @17GHz	0.0012 0.0018 @17GHz
[21]	ABS	$BaTiO_3$	29 vol %	SD	No	8.72@14.13 GHz	0.027 @14.13 GHz
[26]	ABS	$BaSrTiO_3$	15 vol %	SD	No	6.05@5GHz	0.007 @5GHz
[39]	PLA	GNP CNT	6%wt	MM & SD	No	12.73 (ME) @26–37 GHz 11.84(SB) @26–37 GHz	n/a

Table 1.
Comparison of literature results on ceramic-thermoplastic feedstock filaments used for FDM printing of RF and microwave devices.

To begin with mixing rules, think of a homogeneous medium (matrix) with relative dielectric permittivity ε_m and spheroids with relative permittivity ε_f. The volume fraction of filler spheroid particles is denoted as Θ_f, while the arising volume fraction of the matrix is $\Theta_m = 1 - \Theta_f$. ε_{eff} represents the effective permittivity of composite material. It is assumed that both filler and matrix have no dielectric loss and that they do not interact with one another chemically.

3.1 Mixing rules-based models

The analytical bounds of the effective permittivity of a binary lossless sandwich composite in terms of its constituent parts can be computed by considering two

extreme cases of interchanging layers: the first case with the layers being normal to the applied field (**Figure 5b**) and the second case with the layers being tangential to the applied field (**Figure 5a**). The upper bound, which represents parallel model, can be calculated using,

$$\varepsilon_{eff,max} = \varepsilon_m \Theta_m \varepsilon_f \Theta_f \tag{2}$$

The lower bound, which represents series model, can be calculated using,

$$\varepsilon_{eff,min} = \frac{\varepsilon_m \varepsilon_f}{\varepsilon_f \Theta_m + \varepsilon_m \Theta_f} \tag{3}$$

3.1.1 Maxwell-Garnett model

A more accurate equation for predicting dielectric properties can be achieved by the following equation known as Maxwell-Garnett equation [32, 44],

$$\varepsilon_{eff} = \varepsilon_m \left[1 + \frac{3\Theta_f(\varepsilon_f - \varepsilon_m)}{(1-\Theta_f)(\varepsilon_f - \varepsilon_m) + 3\varepsilon_m}\right] \tag{4}$$

This equation considers the dielectric permittivity of spherical fillers scattered in a medium, as illustrated in **Figure 5c**. In the literature, the Maxwell-Garnett equation is represented in a variety of ways and referred to by various other names, including Maxwell-Wagner [48], Rayleigh [49], and Lorentz-Lorenz [50]. One of such Maxwel-Garnett equation forms is given below,

$$\frac{\varepsilon_{eff} - \varepsilon_m}{\varepsilon_{eff} + 2\varepsilon_m} = \Theta_f \left[\frac{\varepsilon_f - \varepsilon_m}{\varepsilon_f + 2\varepsilon_m}\right] \tag{5}$$

This equation applies solely to spherical particles. For dispersed particles that are not spherical in shape, Eq. (5) must be changed. A popular method for including information about the geometry of scattered particles is to incorporate a depolarization factor that is proportional to their divergence from sphericity. Thus, the Maxwell-Garnett model equation (Eq. (4)) could be altered to this form to make it more general [51],

$$\varepsilon_{eff} = \varepsilon_m \left[1 + \frac{\Theta_f(\varepsilon_f - \varepsilon_m)}{D(1-\Theta_f)(\varepsilon_f - \varepsilon_m) + \varepsilon_m}\right] \tag{6}$$

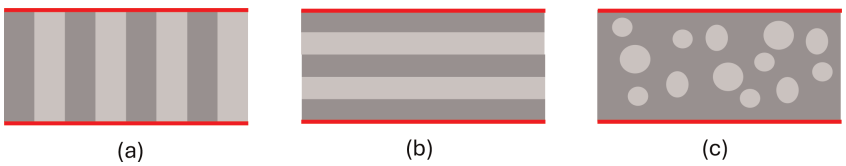

Figure 5.
(a) Parallel model, (b) series model, and (c) mixing model. Red lines are for electrodes.

where parameter D is depolarization factor. For D = 1/3, Eq. (6) simplifies as Eq. (4). Value of D could be computed or can be found in the literature for different geometrical shapes [51].

3.1.2 Lichtenker model

According to Weiner's theory, the lower and upper boundaries are given by eqs. (2) and (3). The higher bound for the effective dielectric permittivity is attained by a system made up of parallel layers arranged tangentially to the applied electric field. The lower bound is achieved by system with the layers that are normal to the applied electrical field. Cross-sectional analysis yields similar results. Starting with eqs. (2) and (3), Lichtenker assumed that the effective dielectric function of the considered composite satisfies the equation:

$$\varepsilon_{eff}^{\alpha} = \varepsilon_f^{\alpha}\Theta_f + \varepsilon_m^{\alpha}\Theta_m \tag{7}$$

where parameter α varies from −1 to 1. The value of −1 for represents anisotropy and value of 1 for α represents isotropy. Each value of α represents a distinct micro-geometrical structure of the composite. One can thus predict that the applicability of Eq. (7) is broader than that of the well-known Maxwell-Garnett equation (Eq. (4)), which, in general, has no free parameters connected to the topology.

3.1.3 Raleigh model

An important advance to the subject matter was made by Lord Rayleigh [52]. The standard assessments of the effective dielectric constant of binary mixes are derived from the Raleigh model. It assumes cylindrical particles mixed in a matrix with effective dielectric constant calculated from the following equation:

$$\frac{\varepsilon_{eff} - \varepsilon_m}{\varepsilon_{eff} + \varepsilon_m} = \Theta_f \left[\frac{\varepsilon_f - \varepsilon_m}{\varepsilon_f + \varepsilon_m}\right] \tag{8}$$

This is quite like Eq. (5). Rayleigh demonstrated that Maxwell's model provides an accurate first-order estimation for cubically ordered spherical and cylindrical fillers in a host matrix. Three things are worth noting: (1) Lord Rayleigh further developed Maxwell's dipole theory [53] of the dispersion of spheres within a medium by considering the contribution of induced octopole moments to conductivity, (2) Rayleigh's model is simpler, but it is equivalent to the Maxwell-Garnett model, and (3) Rayleigh's model revealed an equivalence of electrical conduction and acoustic propagation.

3.1.4 Jaysundere: Smith equation

At greater particle concentrations, the interaction among particles is more important due to the shorter distance between them, as seen in **Figure 6b**. Jaysundere-Smith [45] estimated the electric field with a dielectric sphere contained in a continuous dielectric matrix, considering the polarization of consecutive particles. According to Jaysundere and Smith, effective relative permittivity can be given *via* equation,

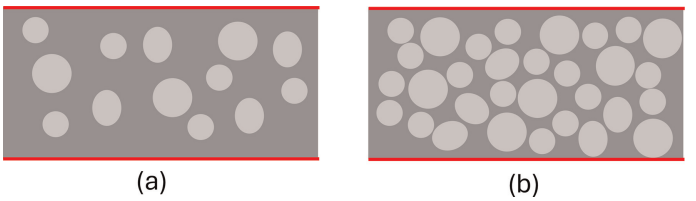

Figure 6.
(a) Composite with lower filler volume fraction and (b) composite with higher filler volume fraction.

$$\varepsilon_{eff} = \frac{\varepsilon_m \Theta_m + \varepsilon_f \Theta_f \left(\frac{3\varepsilon_m}{2\varepsilon_m + \varepsilon_f}\right)\left[1 + 3\Theta_f \frac{(\varepsilon_f - \varepsilon_m)}{2\varepsilon_m + \varepsilon_f}\right]}{\Theta_m + \Theta_f \left(\frac{3\varepsilon_m}{2\varepsilon_m + \varepsilon_f}\right)\left[1 + 3\Theta_f \frac{(\varepsilon_f - \varepsilon_m)}{2\varepsilon_m + \varepsilon_f}\right]} \tag{9}$$

3.2 Effective medium theory-based models

Effective medium theories (EMT) apply when the fields are quasistatic, meaning that the wavelength of the electromagnetic radiation probing the system is substantially larger than the typical scale of inhomogeneities. The frequency also defines the nature of the microscopic mechanisms within a material that govern the bulk material's macroscopic polarization (and magnetization) response. Polarization in materials can be caused by a variety of mechanisms, including electronic, ionic, atomic, dipolar, and interfacial, as detailed in the introduction.

3.2.1 Hanai-Bruggman model

The Bruggeman model [54], which was also developed by Hanai [55], is a popular model for calculating the relative permittivity of EM composites. It is cited as the Hanai-Bruggeman model [56]. One advantage of this model is that it assumes filler particles to be very close to each other; this is indicated by the following equation,

$$\frac{\varepsilon_f - \varepsilon_{eff}}{\varepsilon_f - \varepsilon_m}\left(\frac{\varepsilon_m}{\varepsilon_{eff}}\right)^{\frac{1}{3}} 1 - \Theta_f \tag{10}$$

The Hanai-Bruggeman model can accurately predict permittivities of composites with volume fractions of particles Θ_f up to around 50%, under the assumption that the scattered filler particles in the composite do not create a percolative path across the matrix.

3.2.2 Stroud-Pan model

Stroud and Pan [57] expanded the EMT to finite frequencies, accounting for particle scattering with a full multipole expansion. In their model, composite is thought of as being made of spherical particles for both matrix and filler as shown in **Figure 7**. Effective permittivity of the composite can be calculated using the following equation,

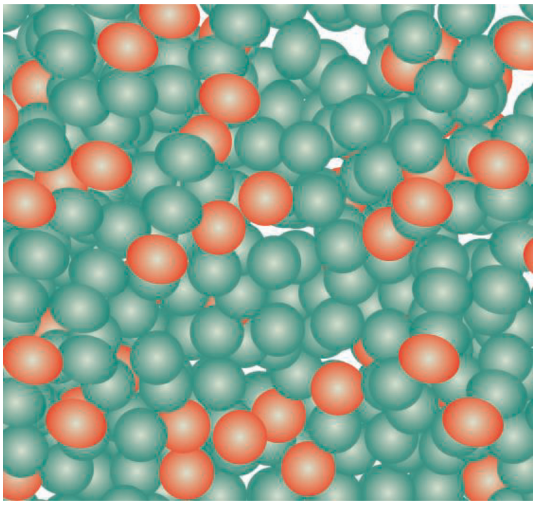

Figure 7.
Composite geometry utilized by Stroud and Pan for computing frequency-dependent permittivity. Red spheres represent filler while green spheres represent matrix representation of fused deposition modeling (FDM) process.

$$\sum_i \Theta_i \left[\frac{\varepsilon_i - \varepsilon_{eff}}{\varepsilon_i + 2\varepsilon_{eff}} + \frac{1}{30} \left(\frac{\omega R_i}{c} \right)^2 (\varepsilon_i - \varepsilon_{eff}) \right] = 0 \tag{11}$$

where Θ_i is the volume fraction of ith material, ε_i is relative permittivity of ith material, R_i is the radius of ith material particles and ω is angular frequency of EM wave and c is speed of light in vacuum.

For the sake of illustration, assume that the composite is made up of only two types of dielectric particles, ε_1 and ε_2, with volume fractions Θ_i and $\Theta_2 = 1 - \Theta_1$, and that each type of particle is formed into approximately spherical shapes of the same radius R. Then eq. (11) assumes the simple form.,

$$\Theta_1 \left[\frac{\varepsilon_1 - \varepsilon_{eff}}{\varepsilon_1 + 2\varepsilon_{eff}} + \gamma(\varepsilon_1 - \varepsilon_{eff}) \right] + \Theta_2 \left[\frac{\varepsilon_2 - \varepsilon_{eff}}{\varepsilon_2 + 2\varepsilon_{eff}} + \gamma(\varepsilon_2 - \varepsilon_{eff}) \right] = 0 \tag{12}$$

where γ equals to $\frac{1}{30}\omega^2 R^2/c^2$. The above equation looks to be a cubic equation for ε_{eff} which simplifies to a prominent quadratic Eq. (5), in the limit (γ = 0).

Different models for predicting the effective dielectric constants of composite materials are compiled and presented to help researchers in developing new high performance ceramic-thermoplastic composite feedstock filaments for fused deposition modeling of RF and microwave devices.

4. Application of FDM printed ceramic-thermoplastic feedstock filaments for RF and microwave applications

As the FDM technology matured and became more available, more researchers in RF and microwave field started using it to 3D print passive RF and microwave devices with complex geometry [58]. The majority of works focused on all-dielectric RF devices, as it is challenging to fabricate smooth conductor surfaces using FDM method [7].

However, there have been advances in research for providing smooth FDM printed conductive surfaces, recently [59, 60].

Given FDM technology's obvious proclivity for printing dielectric materials, most scientific endeavors that use this technique are mainly focused on manufacturing pure dielectric devices such as reflect arrays, dielectric resonator antennas (DRAs), lenses, and dielectric rod antennas (DRAs). Companies such as Preperm [61] and Zetamix [62] are beginning to cater to the specialty material market for FDM printing of RF devices, which will improve the momentum of research publication and potential commercial application.

Although not exhaustive, authors have tried to compile a list of known RF and microwave device applications presented in literature that use ceramic-thermoplastic feedstock filaments for fused deposition modeling. These works are broadly characterized based on whether the material was developed in lab or commercially purchased.

4.1 Laboratory-made ceramic-thermoplastic composites

Castro et al. [31] demonstrated for the first time 3D printed microwave devices employing cyclo-olefin-polymer (COP)-based composites *via* an FDM process. They also observed the highest relative dielectric permittivity value of ~5 and an ultra-low dielectric loss tangent tan (δ_d) < 0.0014 for COP-based composites. **Figure 8a** illustrates how they used 3D printing to create rectangular edge-fed patch antennas operating at around 17 GHz. The substrates for these antennas were 3D printed using 25% v/v COP-$MgCaTiO_2$ ($\boldsymbol{\varepsilon_r}$~4.47) and pure COP ($\boldsymbol{\varepsilon_r}$~2.27). A 49.35% reduction in size was reported for antenna fabricated with 25% v/v COP-$MgCaTiO_2$ compared to edge-fed patch antenna made of pure COP.

Goulas et al. [26] used $BaSrTiO_2$ in acrylonitrile butadiene styrene (ABS) composite ($\boldsymbol{\varepsilon_r}$ ~6.05 and tan (δ_d) ~ 0.007 at 5 GHz) with 15.26 vol% filler to 3D print a prototype microstrip patch 5G antenna and a hemispherical dielectric lens, as shown

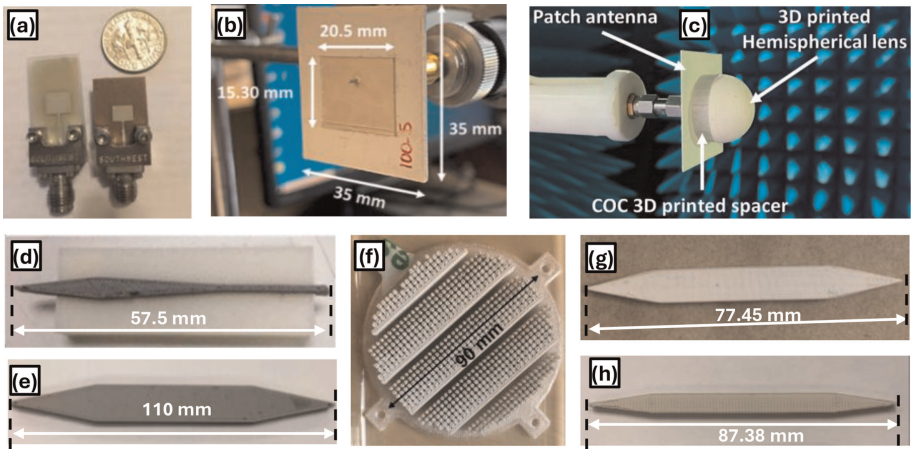

Figure 8.
(a) 3D printed patch antennas over pure COP and 25%v/v COP-$MgCaTiO_2$ substrate [20] (b) microstrip patch 5G antenna on 3D printed 15.26%v/v ABS-$BaSrTiO_2$ substrate [26] (c) hemispherical dielectric lens 3D printed using 15.26%v/v ABS-$BaSrTiO_2$ [26](d) FDM printed DRA using 30%v/v COP- $MgCaTiO_2$ composite filament along with ABS cladding [63](e) FDM printed DRW using 30%v/v COP- $MgCaTiO_2$ composite [64](f) 3D printed subwavelength deflector using 36%v/v COC-TiO_2 composite [27](g)DRW FDM printed using 30%v/v COP- TiO_2 composite filament [30] (h) DRW FDM printed using 40%v/v COP- TiO_2 composite filament [43].

in **Figure 8b** and **c**, respectively. The rectangular microstrip patch was fabricated *via* fused filament fabrication (FFF) 3D printing. A hemispherical dielectric lens with a radius of 25 mm (which fed with a different microstrip patch antenna) was also fabricated using FFF 3D printing using the same composite and a 100% infill setting.

Lugo et al. [63] used COP and $MgCaTiO_2$ (MCT) based composite ($\boldsymbol{\varepsilon_r}$∼4.34 and tan ($\delta_d$) ∼ 0.0060 at 44 GHz), with 30% volume of ceramic filers to FDM print dielectric rod antenna operating in mm-wave frequencies. The peak gain of the multilayer antenna is over 22 dBi for the entire frequency range of 30–40 GHz. **Figure 8d** shows the DRA along with low permittivity (ABS) cladding used to enhance the antenna performance.

In a follow-up paper, they used the same 30 vol. % COP-$MgCaTiO_2$ composite ($\boldsymbol{\varepsilon_r}$ ∼4.82 and tan (δ_d) ∼ 0.0018 at 17 GHz) to fabricate a multilayer dielectric rod waveguide (DRW) for operation at an extended Ku-band from 10 to 18 GHz [64]. The insertion loss of the dielectric rod waveguide stays within 0.01 dB/mm and 0.012 dB/mm, which is comparable to the previously reported multilayer DRW that was constructed from a commercial high-k material not compatible with FDM [64]. **Figure 8e** presents the picture of the 3D-printed DRW made of composite material.

Hoang et al. [27] fabricated a subwavelength deflector using cyclo-olefin copolymer (COC) and TiO_2 composite and compared it to a counterpart 3D printed in ABS. To obtain a high-permittivity and low-loss composite, the TiO_2 ($\boldsymbol{\varepsilon_r}$ ∼ 100, tan (δ_d) < 10^{-4}) was loaded at 36% volume in the low-loss polymer matrix COC (tan (δ_d) < 10^{-3}). The deflectors were intended to refract an incoming plane wave with 0° incidence by 30° at 30 GHz. Using this high-permittivity printed material, the thickness of the 90 mm-diameter subwavelength deflector is reduced by more than twice, the realized gain is increased by 1 dB across the full frequency range of 27.5–31 GHz, and the side lobe level is reduced by 7 dB. **Figure 8f** depicts the 3D manufactured subwavelength deflector. Following laboratory research, the disclosed COC-TiO2 filament has been manufactured on an industrial scale and has been sold since the end of 2022 [62].

The authors used a 30% volume COP-TiO_2 ($\boldsymbol{\varepsilon_r}$ ∼5.37 and tan (δ_d) ∼ 0.003 at 16 GHz) composite to 3D print dielectric rod waveguide operating in the frequency range of 12–18 GHz [30]. FDM printed DWG exhibited an impressive low loss of 0.017 dB/mm at 17.5 GHz. In a follow-up paper, authors fabricated DWGs made from 30% volume COP-TiO_2 and 40% volume COP-TiO_2 ($\boldsymbol{\varepsilon_r}$ ∼6.86 and tan (δ_d) ∼ 0.0019 at 16 GHz) for mm-wave frequencies (Ka and V-bands) [43]. 3D printed DWGs for Ka band and V band are shown in **Figure 8g** and **h**, respectively.

4.2 Commercially available ceramic-thermoplastic composites

Huang et al. took advantage of commercially available dielectric composite filament named PREPERM 3-D ABS DK 10.0 from Premix with relative permittivity $\boldsymbol{\varepsilon_r}$ of 10.0, and loss tangent tan (δ_d) of 0.003, to fabricate different kinds of antenna applications, from dielectric resonator antenna to dielectric rod antenna [65–68]. In [66, 68], they fabricated low-profile end-fire dielectric antennas with wideband performance consisting of four and five dielectric sections designed with tapered permittivities and sizes to achieve impedance-matched surface-wave launching over a wide bandwidth, as shown in **Figure 9a** and **b**. In several of their works, they used 3-D printing technology to regulate the effective permittivity of dielectric blocks in the 2.0 to 8.3 range by altering the fill factor. They also 3-D-printed a dielectric rod antenna

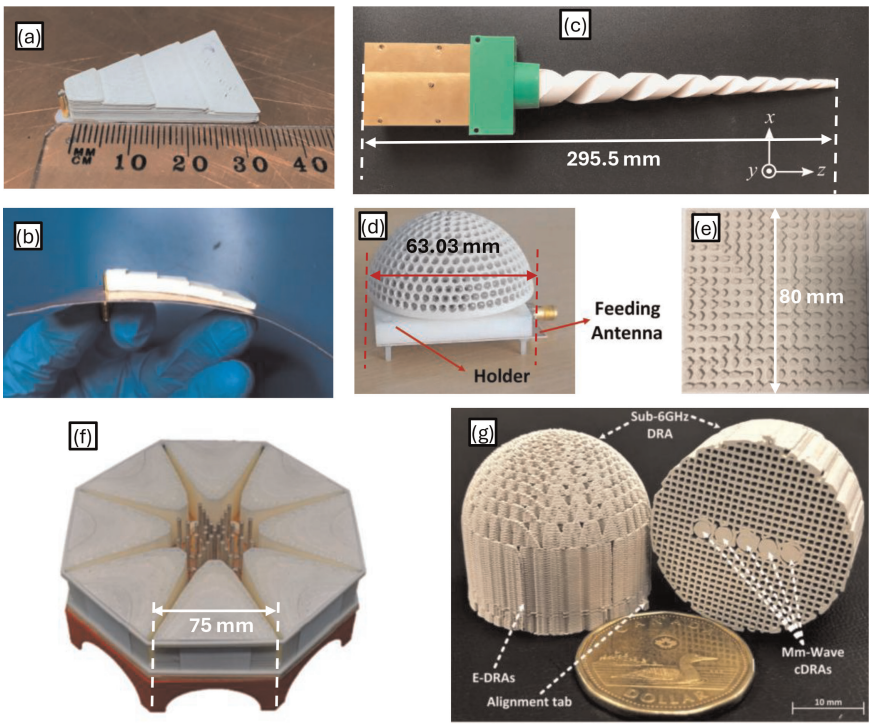

Figure 9.
(a) Low-profile end-fire dielectric antenna [68], (b) conformal low-profile end-fire dielectric antenna [66], (c) dielectric rod antenna with wideband circular polarization using helical grooves in tapered dielectric rod [65], (d) hemispherical lens (18–24 GHz) with circular corrugated matching layer and perforated matching layer regions [69], (e) mm-wave dual-polarized dielectric resonator reflect array [70], (f) gradient-index lens antenna fed by a switched monopole feed array [71], and (g) dual wideband encapsulated dielectric resonator antennas [71].

with wideband circular polarization which used a tapered dielectric rod with two helical grooves (**Figure 9c**) for generating circular polarization.

Alçep and Tokan [69] employed Preperm ABS1000 filament ($\boldsymbol{\varepsilon_r}$ ~10 & tan (δ_d) ~ 0.003) from Premix for 3D printing of hemispherical lens (18–24 GHz) prototype consisting of circular corrugated matching layer and perforated matching layer regions (**Figure 9d**). Instead of the standard broadband matching procedure, which requires the machining of three additional layers of different materials on the lens surface, they employed an alternate matching technique that is feasible to implement with 3D printing technology. The reported performance in terms of beam scanning capability of the perforated lens with 70° scan angle and 2.7 dB scan loss is promising for next-generation automotive radar sensors.

Sun et al. [70] presented a 3D printed millimeter-wave dual-polarized dielectric resonator (DR) reflect array (16 × 16 elements) working in the Ka band. PREPERM 3-D ABS DK 10.0 from Premix materials ($\boldsymbol{\varepsilon_r}$ ~ 10, tan (δ_d) ~ 0.003) was used as the dielectric filament for FDM process. **Figure 9e** shows a picture of the 3D-printed reflect array. The unit cell of the reflect array is composed of two elliptical DRs orthogonally placed in the center. A recorded peak antenna gains of 22.53 dBi was reached, resulting in a gain improvement of 7.43 dB above the feed horn alone.

Giddens and Hao [73] also utilized commercially available standard white ABS from Verbatim and ABS-400 filament from PREPERM with permittivities of 2.69 and 3.99, respectively. They designed and fabricated a gradient-index lens antenna

(**Figure 9f**) designed to radiate with a 45° beamwidth across eight different sectors fabricated by multi-material FDM 3D printing. At 5.8 GHz, the lens antenna was supplied by a switched monopole feed array, resulting in 360° pattern diversity. The lens antenna had a graded dielectric profile from 3.6 down to 1.3.

Malfajani et al. [71] proposed the concept of encapsulated dielectric resonator antennas (EDRAs). E-DRAs are constructed by embedding smaller DRAs with a specified dielectric constant inside a bigger DRA (**Figure 9g**) with a lower dielectric constant, facilitating efficient radiation at two widely spaced and heavily utilized frequency bands. The FFF 3D printing technique is used to fabricate the whole E-DRA structure with a single material (commercial filament PREPERM 3D ABS DK 12.0 from company Avient based in Belgium) but with different infill, percentages to achieve the required permittivity. An array of five elements was employed in a switched mode configuration to add switching beam capability to the antenna in the mm-wave band. The measurement findings depicted a maximum gain of 7.2 dBi at 3.2 GHz and 18 dBi at 31.5 GHz. The calculated efficiency in the sub-6-GHz and mm-wave bands is better than 95% and 80%, respectively. The dielectric constant of the smaller DRA was chosen to be 9, because this is the greatest dielectric constant that can be obtained by ABS1200 through the FFF 3D printing method at mm-wave frequencies.

de Oliveira Neto et al. [72] introduced a technique to produce RF and microwave devices with relative permittivity ($\boldsymbol{\varepsilon_r}$) variations using two or more filaments, with different permittivities, which they introduced into the print head and mixed with designed proportions. They designed and built a dielectric planar lens, with varying permittivity, to work along with a planar antipodal Vivaldi antenna (AVA). Yellow ABS filaments ($\boldsymbol{\varepsilon_r} \sim 2.6$ & tan (δ_d) ~ 0.032) and graphite-filled ABS filaments ($\boldsymbol{\varepsilon_r} \sim 6.5$ & tan (δ_d) ~ 0.36) were used as two feeding materials. As seen in **Figure 10**, they chose the palm tree as the reference antenna for the experiments. Their building process differs from others in the literature in that it creates materials by combining filaments with varying electrical permittivity values.

FDM is foremost and widely utilized AM methods for prototyping EM devices. It's being economical and easy to use, overcome the disadvantages such as lack of thermoplastic materials with extremely high dielectric constant, and the post-processing requirements associated with deposition of (electrically conductive) metallic surfaces.

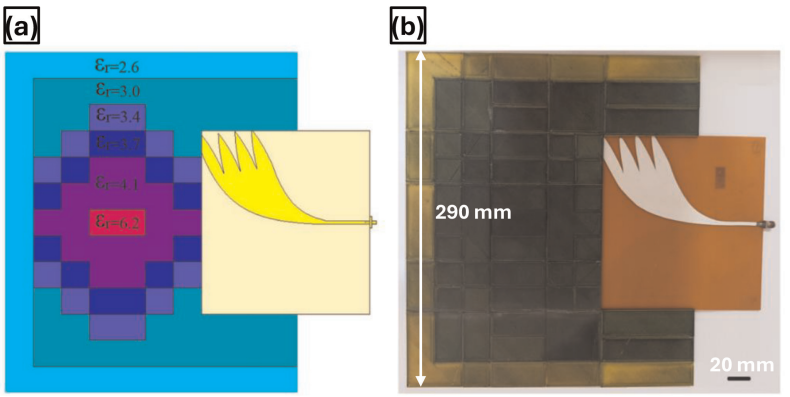

Figure 10.
(a) Simulation model of the lens antipodal Vivaldi antenna with variations of relative permittivity indicated with different colors and (b) picture of 3D printed lens antenna prototype with outermost part composed of yellow ABS and innermost part composed of 95% of graphite-filled ABS [72].

5. Conclusion

Additive manufacturing, especially fused deposition modeling offers feasibility of complex geometries for RF and microwave devices which cannot be achieved or are expensive to achieve using traditional fabrication methods. However, commercially offered 3D printable materials are not optimal for RF and microwave frequencies as they lack high relative permittivity and low-loss-tangents offered by traditional PCB laminates.

Incorporating ceramic filler particles in thermoplastic matrix makes it feasible to combine processibility of thermoplastics with the unique dielectrical properties offered by ceramic materials. Melt mixing is a simpler and more cost-effective way to manufacture ceramic-thermoplastic composites. However, it can only achieve repeatable dispersion of ceramic fillers for composites with up to 30% filler volume fraction. Solution-assisted dispersion can achieve repeatable dispersion of ceramic fillers for higher volume fraction compared to melt mixing. However, it requires expensive and sometimes hazardous chemical solvents, which makes it more expensive. Both above-mentioned methods can be enhanced by incorporating a surface treatment of ceramic fillers before dispersing them in thermoplastic matrix. Surfactant can serve the dual purpose of hindering filler particle agglomeration and improving the interface between filler and matrix.

In this chapter, different methodologies of fabricating ceramic-thermoplastic feedstock filaments are reviewed, and their application for FDM printing of RF and microwave devices is presented. Widely used analytical prediction models for predicting the effective permittivity of the composite materials are listed. Given the limitless and high potential applications of 3-D printing, ongoing research, particularly FDM printed composites, should be encouraged and pursued. The use of microparticles has been shown to generate and build more functional products. It is critical to continue the development of new materials that are precisely tuned for certain electromagnetic applications.

Acknowledgements

This work was supported by NSF grant award number 2329207, entitled "Collaborative Research: FuSe: Thermal Co-Design for Heterogeneous Integration of Low Loss Electromagnetic and RF Systems (The CHILLERS)".

Author details

Vishvajitsinh Kosamiya* and Jing Wang
Department of Electrical Engineering, University of South Florida (USF), Tampa, United States

*Address all correspondence to: vkkosamiya@ieee.org

References

[1] Clark RH. Handbook of Printed Circuit Manufacturing. Netherlands: Springer; 2012

[2] Ferrando-Rocher M, Herranz-Herruzo JI, Valero-Nogueira A, Bernardo-Clemente B. Performance assessment of gap-waveguide Array antennas: CNC milling versus three-dimensional printing. IEEE Antennas and Wireless Propagation Letters. 2018; **17**:2056-2060

[3] Koul SK, Swapna S, Karthikeya GS. Additive manufacturing in antenna development. In: Koul SK, Swapna S, Karthikeya GS, editors. Antenna Systems for Modern Wireless Devices. Singapore: Springer Nature Singapore; 2024. pp. 283-319

[4] Karthikeyan SS, Mellita RA. Additive manufacturing of MTM-FSS. In: Narayan S, Kesavan A, editors. Handbook of Metamaterial-Derived Frequency Selective Surfaces. Singapore: Springer Nature Singapore; 2022. pp. 695-720

[5] Mazzei, Capote GA, Montoya-Ospina MC, Liu Z, Mattei MS, Liu B, Delgado AP, et al. Compounding a high-permittivity thermoplastic material and its applicability in manufacturing of microwave photonic crystals. Materials (Basel). 2022;**15**(7):1-15

[6] Wang Y, Zhang X, Su R, Chen M, Shen C, Xu H, et al. 3D printed antennas for 5G communication: Current progress and future challenges. Chinese Journal of Mechanical Engineering: Additive Manufacturing Frontiers. 2023;**2**(1): 100065

[7] Chietera FP. Additively manufactured antennas and electromagnetic devices. Hardware. 2024;**2**(2):85-105

[8] Liu R, Mumcu G, Wang J, editors. Towards additive manufacturing based packaging of mm-wave antenna arrays and Beamformer ICs. In: 2024 IEEE Wireless and Microwave Technology Conference (WAMICON). Clearwater, FL, USA: IEEE; 2024. pp. 15-16

[9] Firat OF, Wang J, Weller T. Characterization of additively manufactured suspended finite ground CPW interconnects enhanced by femtosecond laser micromachining. IEEE Transactions on Components, Packaging and Manufacturing Technology. 2024;**14**(6):965-972

[10] Liu R, Braun J, Mitchell G, Wang J, Mumcu G, editors. Packaging of a beamforming IC by laser enhanced direct print additive manufacturing (LE-DPAM). In: 2022 3rd URSI Atlantic and Asia Pacific Radio Science Meeting (AT-AP-RASC); 30 May-4 June 2022. Gran Canaria, Spain: IEEE; 2022

[11] Firat OF, Wang J, Weller T. Additively manufactured metal-insulator-metal capacitors using a high-K dielectric paste. In: 2022 IEEE International Symposium on Antennas and Propagation and USNC-URSI Radio Science Meeting (AP-S/URSI); 10–15 July 2022. Denver, CO, USA: IEEE; 2022

[12] Firat O, Wang J, Weller T, editors. Laser-assisted and additively manufactured multilayer metal-insulator-metal capacitors. In: 2022 IEEE 22nd Annual Wireless and Microwave Technology Conference (WAMICON). Clearwater, FL, USA: IEEE; 2022. pp. 27-28

[13] Abdin MM, Johnson WJD, Wang J, Weller TM. W-band MMIC Chip assembly using laser-enhanced direct print additive manufacturing. IEEE

Transactions on Microwave Theory and Techniques. 2021;**69**(12):5381-5392

[14] Ahmadloo M. Design and fabrication of geometrically complicated multiband microwave devices using a novel integrated 3D printing technique. In: 2013 IEEE 22nd Conference on Electrical Performance of Electronic Packaging and Systems. San Jose, CA, USA: IEEE; 2013

[15] Peverini OA, Addamo G, Lumia M, Virone G, Calignano F, Lorusso M, et al. Additive manufacturing of Ku/K-band waveguide filters: A comparative analysis among selective-laser melting and stereo-lithography. IET Microwaves, Antennas & Propagation. 2017;**11**(14): 1936-1942

[16] Zacharatos F, Theodorakos I, Karvounis P, Tuohy S, Braz N, Melamed S, et al. Selective laser sintering of laser printed Ag nanoparticle micropatterns at high repetition rates. Materials. 2018;**11**(11):2142

[17] Shamvedi D. Design of Microwave Components Using Direct Metal Laser. Sintering: Waterford Institute of Technology; 2018

[18] Rodrigues ASL, Pires ACB, Barbosa PA, Silveira ZC. Polymeric composites in extrusion-based additive manufacturing: A systematic review. Polymer Composites. 2024;**45**(8): 6741-6770

[19] Mogan J, Harun WSW, Kadirgama K, Ramasamy D, Foudzi FM, Sulong AB, et al. Fused deposition modelling of polymer composite: A progress. Polymers [Internet]. 2023;**15**(1):1-27

[20] Castro J, Rojas E, Ross A, Weller T, Wang J. High-k and low-loss thermoplastic composites for fused deposition modeling and their application to 3D-printed Ku-band antennas. In: 2016 IEEE MTT-S International Microwave Symposium (IMS); 22–27 May 2016. San Francisco, CA, USA: IEEE; 2016

[21] Castles F, Isakov D, Lui A, Lei Q, Dancer CE, Wang Y, et al. Microwave dielectric characterisation of 3D-printed $BaTiO_3$/ABS polymer composites. Scientific Reports. 2016;**6**:22714

[22] Mirzavand R, Honari MM, Aslanzadeh S, Saghlatoon H, Mousavi P. Evaluation of one-staged 3-D printed frequency selective surface using carbon-fiber-reinforced thermoplastic composite. IEEE Transactions on Components, Packaging and Manufacturing Technology. 2019;**9**(11): 2298-2304

[23] Li M. Additively Manufactured Electronic Devices and Antennas for Microwave and Millimeter-Wave 5G Applications. Ultimo, NSW, Australia: University of Technology Sydney; 2023

[24] Lumia M, Addamo G, Virone G, Peverini OA, Paonessa F, Rabitsch J, et al. RF characterization of 3D-printed dielectric materials. In: 2023 IEEE Conference on Antenna Measurements and Applications (CAMA); 15–17 Nov. 2023. Genoa, Italy: IEEE; 2023

[25] García CS, Bedia B, Palczynski G, Godja N, Seidler K, Gorsche C. Polymer-based additive manufacturing of a complex RF front-end for new space applications. In: 2024 18th European Conference on Antennas and Propagation (EuCAP); 17–22 March 2024. Glasgow, United Kingdom: IEEE; 2024

[26] Goulas A, McGhee JR, Whittaker T, Ossai D, Mistry E, Whittow W, et al. Synthesis and dielectric characterisation of a low loss $BaSrTiO_3$/ABS ceramic/polymer composite for fused filament

fabrication additive manufacturing. Additive Manufacturing. 2022;**55**: 102844-102852

[27] Hoang TQV, Vandelle E, Czarny R, Loiseaux B, Fournier T, Penin N, et al. Benefits of using a high-permittivity and low-loss printable material for sub-wavelength deflectors. In: 2023 IEEE Conference on Antenna Measurements and Applications (CAMA) 2023. Genoa, Italy: IEEE; 2023. pp. 492-496

[28] Packard H. Basics of Measuring the Dielectric Properties of Materials. Application Note 1217–1 [Internet]. Palo Alto, CA: Hewlett Packard; 1992

[29] Castro J, Rojas-Nastrucci EA, Ross A, Weller TM, Wang J. Fabrication, modeling, and application of ceramic-thermoplastic composites for fused deposition modeling of microwave components. IEEE Transactions on Microwave Theory and Techniques. 2017;**65**(6):2073-2084

[30] Kosamiya V, Wang J, editors. High-k and low-loss dielectric composite feedstock filaments, tailored for additive manufacturing of microwave devices. In: 2020 IEEE/MTT-S International Microwave Symposium (IMS); 4–6 Aug 2020. Los Angeles, CA, USA: IEEE; 2020

[31] Castro JDD. Engineered Nanocomposite Materials for Microwave/Millimeter-Wave Applications of Fused Deposition Modeling. Tampa, FL, USA: University of South Florida; 2017

[32] Dang Z-M, Yuan J-K, Zha J-W, Zhou T, Li S-T, Hu G-H. Fundamentals, processes and applications of high-permittivity polymer–matrix composites. Progress in Materials Science. 2012;**57**(4):660-723

[33] Todd MG, Shi FG. Complex permittivity of composite systems: A comprehensive interphase approach. IEEE Transactions on Dielectrics and Electrical Insulation. 2005;**12**(3):601-611

[34] Vo HT, Shi FG. Towards model-based engineering of optoelectronic packaging materials: Dielectric constant modeling. Microelectronics Journal. 2002;**33**(5–6):409-415

[35] Kim H, Abdala AA, Macosko CW. Graphene/polymer nanocomposites. Macromolecules. 2010;**43**(16):6515-6530

[36] Lee J-Y, An J, Chua CK. Fundamentals and applications of 3D printing for novel materials. Applied Materials Today. 2017;**7**:120-133

[37] Martin C. Twin screw extruders as continuous mixers for thermal processing: A technical and historical perspective. AAPS PharmSciTech. 2016; **17**(1):3-19

[38] Kattel B, Ayan U, Mohoppu M, Villacorta B, Hutchcraft WE. Enhancing permittivity of 3D printing filaments via Nanocompounding for electromagnetic applications. In: SoutheastCon 2024; 15–24 March 2024. Atlanta, GA, USA: IEEE; 2024

[39] Adami R, Lamberti P, Bychanok D, Kuzhir P, Tucci V. Electromagentic Properties of Filaments Containing Nanofillers for 3D Printing. Milano, Italy: Italian Association of Chemical Engineering; 2021

[40] Khatri B, Lappe K, Habedank M, Mueller T, Megnin C, Hanemann T. Fused deposition modeling of ABS-barium titanate composites: A simple route towards tailored dielectric devices. Polymers (Basel). 2018;**10**(6):1-18

[41] Wu Y, Isakov D, Grant PS. Fabrication of composite filaments with high dielectric permittivity for fused

deposition 3D printing. Materials (Basel). 2017;**10**(10):1-11

[42] Parsons P, Larimore Z, Mirotznik M, Mitchell G. Composite materials development for fused filament fabrication of RF systems. In: 2020 International Applied Computational Electromagnetics Society Symposium (ACES); 27–31 July 2020. Basel, Switzerland: MDPI; 2017

[43] Kosamiya V, Wang J. Composite feedstock filaments for fused deposition modeling (FDM) of microwave interconnects. IEEE Transactions on Components, Packaging and Manufacturing Technology. 2023;**13**(2): 249-256

[44] Garnett JCM, XII LJ. Colours in metal glasses and in metallic films. Philosophical Transactions of the Royal Society of London Series A, Containing Papers of a Mathematical or Physical Character. 1997;**203**(359–371):385-420

[45] Jayasundere N, Smith BV. Dielectric constant for binary piezoelectric 0-3 composites. Journal of Applied Physics. 1993;**73**(5):2462-2466

[46] Czarny R, Hoang TQVTQ, Loiseaux B, Bellomonte G, Lebourgeois R, Leuliet A, et al. High permittivity, low loss, and printable thermoplastic composite material for RF and microwave applications. In: 2018 IEEE Conference on Antenna Measurements & Applications (CAMA); 3–6 Sept. 2018. Västerås, Sweden: IEEE; 2018

[47] Brosseau C. Modelling and simulation of dielectric heterostructures: A physical survey from an historical perspective. Journal of Physics D: Applied Physics. 2006;**39**(7):1277-1294

[48] Wagner K. The after effect in dielectrics. Archiv fur Elektrotechnik. 1914;**2**(378):e394

[49] Nelson SO, You TS. Relationships between microwave permittivities of solid and pulverised plastics. Journal of Physics D: Applied Physics. 1990;**23**(3): 346

[50] Shen LC, Savre WC, Price JM, Athavale K. Dielectric properties of reservoir rocks at ultra-high frequencies. Geophysics. 1985;**50**(4):692-704

[51] Nan C-W. Physics of inhomogeneous inorganic materials. Progress in Materials Science. 1993;**37**(1):1-116

[52] Rayleigh L. On the influence of obstacles arranged in rectangular order upon the properties of a medium. Phiiris Mag. 1892;**34**(481):507

[53] Maxwell JC. A Treatise on Electricity and Magnetism. Oxford, UK: Clarendon Press; 1873

[54] Burggeman D. Calculation of various physics constants in heterogeneous substances I. Dielectricity constants and conductivity of mixed bodies from isotropic substances. Annalen der Physik. 1935;**24**:626-664

[55] Hanai T. Theory of the dielectric dispersion due to the interfacial polarization and its application to emulsions. Kolloid-Zeitschrift. 1960; **171**(1):23-31

[56] Zhou W, Hinojosa BB, Nino JC, Petrovsky V. Applicability of the Bruggeman equation for analyzing dielectric slurries containing ceramic powders with high permittivity. Journal of the American Ceramic Society. 2011; **95**(2):457-460

[57] Stroud D, Pan FP. Self-consistent approach to electromagnetic wave propagation in composite media: Application to model granular metals. Physical Review B. 1978;**17**(4):1602-1610

[58] Munina I, Grigoriev I, O'Donnell G, Trimble D. A review of 3D printed gradient refractive index lens antennas. IEEE Access. 2023;**11**:8790-8809

[59] Colella R, Chietera FP, Michel A, Muntoni G, Casula G, Montisci G, et al. Electromagnetic characterisation of conductive 3D-printable filaments for designing fully 3D-printed antennas. IET Microwaves, Antennas & Propagation. 2022;**16**(11):687-698

[60] Colella R, Chietera FP, Muntoni G, Casula GA, Montisci G, Catarinucci L. Evaluating the effectiveness of planar and waveguide 3D-printed antennas manufactured using dielectric and conductive filaments. IEEE Access. 2023; **11**:34891-34898

[61] Preperm. [Online]. 2019 [Preperm webpage on 3D filaments; [Online]. Available from: https://www.preperm.com/webshop/product-category/3dfilaments

[62] [Online]. Online: Nanoe; 2024 [zetamix]. Available from: https://zetamix.fr/use-case/metasurface-for-flat-antennas/

[63] Lugo DC, Ramirez RA, Castro J, Wang J, Weller TM. 3D printed multilayer mm-wave dielectric rod antenna with enhanced gain. In: 2017 IEEE International Symposium on Antennas and Propagation & USNC/URSI National Radio Science Meeting; 9–14 July 2017. San Diego, CA, USA: IEEE; 2017

[64] Lugo DC, Ramirez RA, Castro J, Wang J, Weller TM. Ku-band additive manufactured multilayer dielectric rod waveguide. In: 2017 IEEE 18th Wireless and Microwave Technology Conference (WAMICON); 24–25 April 2017. Cocoa Beach, FL, USA: IEEE; 2017

[65] Huang J, Chen SJ, Xue Z, Withayachumnankul W, Fumeaux C. Wideband circularly polarized 3-D printed dielectric rod antenna. IEEE Transactions on Antennas and Propagation. 2020;**68**(2):745-753

[66] Huang J, Chen SJ, Xue Z, Withayachumnankul W, Fumeaux C. Wideband 3D printed conformal dielectric antenna with end-fire radiation. In: 2019 IEEE International Symposium on Antennas and Propagation and USNC-URSI Radio Science Meeting; 7–12 July 2019. Atlanta, GA, USA: IEEE; 2019

[67] Huang J, Chen SJ, Xue Z, Withayachumnankul W, Fumeaux C. Impact of infill pattern on 3D printed dielectric resonator antennas. In: 2018 IEEE Asia-Pacific Conference on Antennas and Propagation (APCAP); 5–8 Aug 2018. Auckland, New Zealand: IEEE; 2018

[68] Huang J, Chen SJ, Xue Z, Withayachumnankul W, Fumeaux C. Wideband endfire 3-D-printed dielectric antenna with designable permittivity. IEEE Antennas and Wireless Propagation Letters. 2018;**17**(11): 2085-2089

[69] Alçep M, Tokan F. Impedance matching technique with perforated, inhomogeneous layers for broadband dielectric lenses. IEEE Sensors Journal. 2021;**21**(18):20018-20026

[70] Sun YX, Wu D, Ren J. Millimeter-wave dual-polarized dielectric resonator reflectarray fabricated by 3D printing with high relative permittivity material. IEEE Access. 2021;**9**: 103795-103803

[71] Malfajani RS, Niknam H, Bodkhe S, Therriault D, Laurin JJ, Sharawi MS. A 3D-printed encapsulated dual wide-band

dielectric resonator antenna with beam switching capability. IEEE Open Journal of Antennas and Propagation. 2023;**4**: 492-505

[72] de Oliveira Neto AM, Justo JF, Beccaro W, de Oliveira AM. Designing and building radio frequency devices with tailored dielectric properties using additive manufacturing. Microwave and Optical Technology Letters. 2023;**65**(3): 777-784

[73] Giddens H, Hao Y. Multibeam graded dielectric lens antenna from multimaterial 3-D printing. IEEE Transactions on Antennas and Propagation. 2020;**68**(9):6832-6837